World Academy of Science, Engineering and Technology
International Journal of Mechanical and Mechatronics Engineering
Vol:17, No:7, 2023

Effect of Exit Annular Area on the Flow Field Characteristics of an Unconfined Premixed Annular Swirl Burner

Vishnu Raj, Chockalingam Prathap

Abstract—The objective of this study was to explore the impact of variation in the exit annular area on the local flow field features and the flame stability of an annular premixed swirl burner (unconfined) operated with a premixed n-butane air mixture at an equivalence ratio (Φ) = 1, 1 bar, and 300K. A swirl burner with an axial swirl generator having a swirl number of 1.5 was used. Three different burner heads were chosen to have the exit area increased from 100%, 160%, and 220% resulting in inner and outer diameters and cross-sectional areas as (1) 10 mm & 15 mm, 98 mm^2 (2) 17.5 mm & 22.5 mm, 157 mm^2 and (3) 25 mm & 30 mm, 216 mm^2. The bulk velocity and Reynolds number based on the hydraulic diameter and unburned gas properties were kept constant at 12 m/s and 4000. (i) Planar Particle Image Velocimetry (PIV) with TiO_2 seeding particles and (ii) CH* chemiluminescence was used to measure the velocity fields and reaction zones of the swirl flames at 5 Hz, respectively. Velocity fields and the jet spreading rates measured at the isothermal and reactive conditions revealed that the presence of a flame significantly altered the flow field in the radial direction due to the gas expansion. Important observations from the flame measurements were: the height and maximum width of the recirculation bubbles normalized by the hydraulic diameter, and the jet spreading angles for the flames for the three exit area cases were: (a) 4.52, 1.95, 34°, (b) 6.78, 2.37, 26°, and (c) 8.73, 2.32, 22°. The lean blowout (LBO) was also measured, and the respective equivalence ratios were: 0.80, 0.92, and 0.82. LBO was relatively narrow for the 157 mm^2 case. For this case, PIV measurements showed that Turbulent Kinetic Energy and turbulent intensity were relatively high compared to the other two cases, resulting in higher stretch rates and narrower LBO.

Keywords—Chemiluminescence, jet spreading rate, lean blow out, swirl flow.

I. Introduction

MANY combustion-based technologies are designed to take advantage of the high consumption rate of rapid, turbulent fuel-air streams in order to achieve large power outputs [7]. However, the large reactant flow rates limit the conditions in which flame stabilization is achievable. The introduction of a recirculation zone (RCZ) is one method for establishing a stable flame in which recirculating hot burnt gases lead to the generation of continuous ignition of unburned reactants in the flow field. RCZ can be accomplished using a physical obstacle in the flow (a bluff body) or swirl conditions in the flow are another method often employed in practical engines. Understanding and forecasting the blow-off mechanism is critical for modelling and developing realistic combustion systems that use bluff bodies and swirl conditions to stabilize flames, such as industrial burners, gas turbines, ramjets, and afterburner combustors.

Vishnu Raj and Chockalingam Prathap are with Department of Aerospace Engineering, Indian Institute of Space Science and Technology, Kerala, Pin 695547 India (e-mail: rjvishnu15@gmail.com, prathapc@iist.ac.in).

Flow past different bluff body geometries and combinations have previously been examined. The RCZ length in swirl stabilised flows is commonly acknowledged to have a significant influence on flame stability and residence time distribution, which can significantly alter soot and NOx formation in the flame [15]. Multiple variables can influence the flow structure and hence the length of the RCZ. The bluff-body size, placement, burner and combustor confinement ratios, burner blockage ratio, and burner shape are among them. For instance, [18] evaluated the influence of the blockage ratio and discovered that increasing the blockage ratio enhanced the RCZ length. Furthermore, [16] revealed that adjusting the confinement ratio, which is the area blocked by the bluff body from the approaching co-flow stream, had no influence on the RCZ length or flame structure. According to [17], increasing the blockage ratio, like increasing the momentum flux ratio of the fuel and air, would shift the reaction zone to the inner side of the RCZ. The effects of the bluff-body flame holders' form and position on the flame structure were also investigated and reported [12], [13], [19]. Most of the investigations are focused on the influence of bluff body size on flame structure. Each author employs a distinct burner for their research. The effect of the nozzle annular area has received little attention.

Building on these previous studies, the current study aims to investigate the impact of nozzle annular exit area on a bluff-body stabilized flame during an extinction event and at stoichiometry, specifically, the influence of increasing annular area on flame stability. By holding all other parameters constant (swirl number, equivalence ratio, fuel composition, exit velocity, and hydraulic diameter), the desirable turbulent swirling flow field characteristics such as turbulence intensities, jet spread angle, reverse mass flow rate, and integral length scales were determined to support the investigation. The flame front under-reacting flow conditions were determined using the CH* chemiluminescence technique. The results of this investigation will contribute to a better understanding of the flame's stability in relation to the scaling of the annular exit area. Furthermore, the effect of higher turbulence levels on such systems will stimulate the knowledge of flame stability within highly turbulent combustion technologies.

II. Experimental Methods

A. Burner Rig and Operating Conditions

To investigate the influence of burner annular area on turbulence levels, a swirl-stabilized axisymmetric annular burner is developed and built. The burner design for this work is a customized version of the burner used by [14]. The swirl burner was made of 5 different parts made of stainless steel as represented in Fig. 1 (Swirler and perforated sheet are retrofitted). The overall height of the burner is 100mm. A converging nozzle is designed to avoid flashbacks. The fuel (n-butane) and air are premixed prior to the burner inlet. Perforated sheets were additionally placed inside the burner to have a uniform flow upstream of the burner.

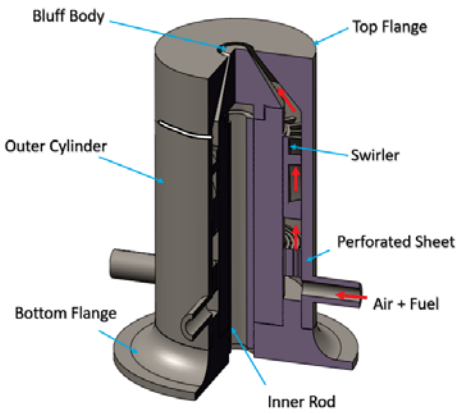

Fig. 1 One quarter cross-section of swirl burner

The experiments were conducted at atmospheric pressure (Unconfined flame). The Reynolds number (based on the exit area of the burner and air/fuel properties) was maintained at 4000 for different burner exit geometries, as shown in Table II by changing the flow rates of the air/fuel mixture by using mass flow controllers (Alicat MFC 0-500 SLPM for air and 0-50 SLPM for fuel). The flow rate uncertainty was estimated to be less than $\mp 0.1\%$ of the maximum flow rate. The top flange and bluff body were only replaced for different operating conditions. The bluff body sizes are selected based on the multiples of hydraulic diameter. Fig. 3 represents the schematic of the experimental setup. The air stream is supplied by an 18.5 kW compressor to a buffer tank of 0.5 m^3 volume capacity through a dehumidifier. The buffer tank ensures a stable flow of air to the test rig. The pressure along the airline is maintained at 2 bar (upstream of MFC) to drive the flow.

The swirling motion introduced by swirl generators was used to get better stabilization of the flame [1], [8]. An axial swirl generator (SS304) with S1.5 was used for all experiments to investigate the effect of the change in the annular exit area. The schematic of the axial swirler is shown in Fig. 2. The details of the swirl generator are shown in Table I. The swirl intensity is defined on the basis of swirl number S, which is specified as the ratio of the axial flux of tangential momentum to the axial flux of axial momentum and a characteristic radius. The expression of the swirl number depends on the swirler geometry and blade profiles [1], which is defined below.

$$S = \frac{G_t}{RG_x} = \frac{2}{3}\left\{\frac{1-\left(R_{h/R}\right)^3}{1-\left(R_{h/R}\right)^2}\right\}\tan\theta \quad (1)$$

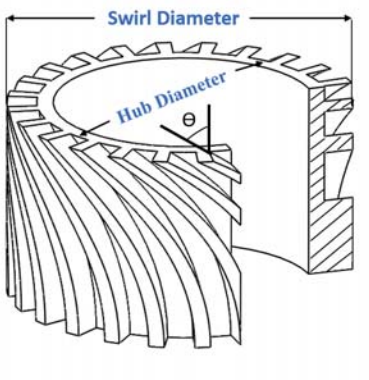

Fig. 2 Quarter section CAD model of axial swirl generator

TABLE I
Specification of Axial Swirl Generator Made of SS304

Sl.No	Parameters	S=1.5
1	Vane Angle- θ (deg)	60
2	Swirler Radius- R (mm)	28
3	Hub Radius- R_h (mm)	22.5
4	Length- L (mm)	30
5	No of Vanes– n	24
6	Thickness of Vanes (mm)	2

B. Particle Image Velocimetry

The instantaneous flow field downstream to the exit of the burner was visualized using the 2D PIV technique consisting of a double pulse Nd-YAG laser (Quantel 200), 2048x2048 CCD camera (Lavision Imager Pro X), and a synchronizing unit (Lavision PTU-X). Fig. 3 shows the schematic of the 2D PIV experimental setup. The pointed laser emitted by the Nd-YAG laser was transformed into a diverging planar sheet with the help of Lavision sheet optics, which subsequently reshaped into a parallel sheet by passing along a collimator. The thickness of the sheet was ensured at approximately 1 mm at the flow field region. The overall height of the region of interest was 60 mm. The laser beam is passed 2 mm above the burner exit to hinder the reflections from the burner surface. TiO_2 having an average diameter less than 5 μm was used as a seeding particle for both isothermal and reacting cases. The camera was equipped with a Nikkor 105 mm focal length lens and a narrow bandwidth optical filter admitting the laser emission 532 $\mp$10 nm and avoiding the emissions from the flame. The distance between the camera and test rig is adjusted to get a better magnification factor, thus improving the accuracy of PIV measurements [10]. The PIV setup was controlled using Davis 8 software, and the MIE scattering data was captured at 5 Hz. The delay between the laser pulses varied between 8-16μs based on the experimental conditions shown in Table II.

The field of view was limited to a 50 mm × 50 mm window centred on the centerline of the flame, yielding a

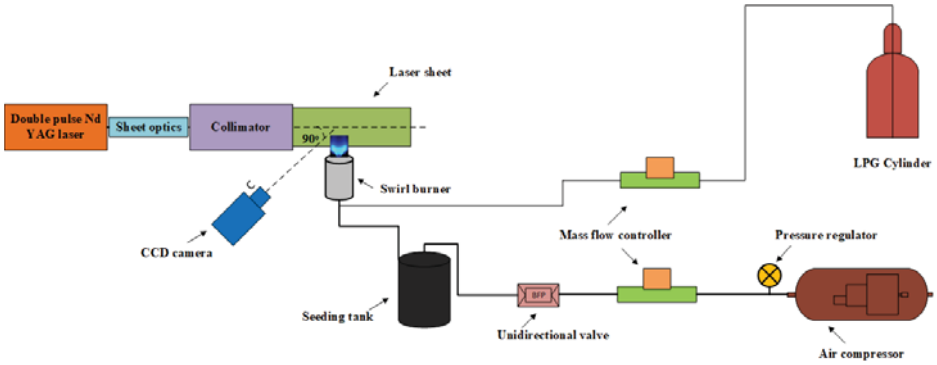

Fig. 3 Schematic of 2D PIV experimental setup

resolution of 28.65 pixels per mm. At a 5Hz acquisition rate, 450 instantaneous images were captured. Using Davis10 software, the PIV pictures are processed to provide the velocity vector field. The instantaneous images were processed using a cross-correlation algorithm with varying interrogation window sizes; a final interrogation window size of 32 x 32 pixels and 50% overlap was used. The spatial distribution of average velocity and turbulent characteristics were estimated based on the radial and axial velocity fields.

C. Direct Photography and Chemiluminescence

The flame's broadband chemiluminescence was captured with a Sony α58 camera with a high spatial resolution (1920 x 1080 pixels, focal length f = 50 mm) and an exposure time of 0.01 s. As indicated, direct flame pictures can be utilized to provide information about the global characteristics of flames, size, shape, colour, and flame stability can sometimes be obtained using a light intensifier. The flame colours of n-butane-air premixed flames can also be used to better understand fuel and air mixing.

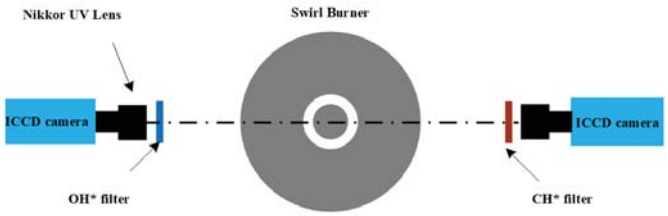

Fig. 4 Schematic of chemiluminescence experimental setup

The spatial distribution of the OH* and CH* chemiluminescence signals from premixed n-butane flames was shown in Fig. 4 using an ICCD camera (Nanostar) which qualitatively measured the localised heat release zone for all. The 105 mm Nikon UV lens (f/4.0) on the ICCD camera provides an image resolution of 1280 x 1024 pixels and a spatial resolution of 100 mm x 100 mm. The OH* and CH* chemiluminescence signals were captured using a band-pass filter with a 40 mm size and a centre wavelength range of 310 nm $\pm$ 2 nm and 430 nm $\pm$ 2 nm, respectively. For comparison, the image intensifier's gate timing was maintained constant at 1 ms, and all instances had identical gain and gate timing parameters. To study the flame structure and response zone of premixed flames, 100 pictures of OH* and CH* are captured at a frequency of 5 Hz and corrected for background intensity before being temporally averaged from 100 images. The time-averaged OH* and CH* chemiluminescence flame images are deconvoluted using the Abel transform to produce CH*/OH* data at the burner's midplane.

III. Results and Discussion

A. Turbulent Flow Field Comparison

Fig. 5 shows the contour plot of one-half of the velocity vector field along with the streamline of three different burners having the exit area increased from left to right (specifications in Table II). The radial and axial distances are normalized with the hydraulic diameter (5 mm). To avoid the disturbances induced due to the laser light reflections on the burner surface, the flow regime between z = 0-2 mm was omitted. The z-axis in Fig. 5 began at 2 mm. Figs. 5 (1a-3a) show the velocity field of air at isothermal condition, Re = 4000, V_{Exit} = 12 m/s, D_h=5 mm, bluff body diameter (BBD) = 10, 17.5, and 25 mm. The present burner has a converging exit, as shown in Fig. 1. At BBD = 10 mm, the exit flow field gradually diverged from its exit onwards, and the effect of the convergent section was absent. As the bluff body size increased, say 17.5 mm and 25 mm, the exit flow initially converged due to the burner's exit geometry, resulting in RCZ behind the BB (BB-RCZ). All three flow fields exhibited a strong central recirculation zone (CRCZ) downstream of BB-RCZ due to the swirling flow. The origin point of the CRCZ shifted downstream with an increase in the BBD and the size of BB-RCZ. The present flame configuration was unconfined; hence, the corner recirculation zones were weak. At isothermal conditions, the flow field was not completely axisymmetric. To have a direct comparison, one-half of the velocity field was shown along with the reacting flow vector fields.

Figs. 5 (1b-3b) show the velocity field of premixed stoichiometric n-butane-air flames. Reynolds number was kept constant identical to that of isothermal condition. The presence of a flame added resistance to the exit flow field resulting in a

complete axisymmetric and streamlined flow field as shown in Fig. 5. In reacting flows, the flow at the exit converged at all bluff-body sizes, resulting in two RCZs similar to isothermal flows. The size and strength of both the RCZ increased with an increase in the BBD due to the associated increase in the mass and momentum flow rates of the reactants. Only the turbulence levels were increased, but the flame temperature remained constant as the combustible mixture remained stoichiometric. Another exciting feature demonstrated in Fig. 5 (1-3) was that the streamline curvature within the CRCZ increased along with the increase in the size of the bluff body while the other parameters remained constant. As streamline curvature enhanced, the adverse pressure gradient also hiked [16], which increased the recirculation mass flow rate. Comparing reacting flow to the isothermal flow showed that the density shift caused the reaction flow's velocity to increase and increased the RCZ mass flow rate [2].

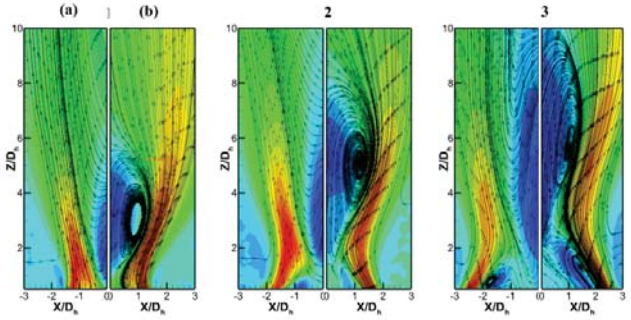

Fig. 5 Streamline superimposed on time-averaged velocity contour for different bluff body sizes. (1) BB10-HD5; (2) BB17.5-HD5; (3) BB25-HD5;. Left part in (1), (2), and (3): Isothermal flow; right part in (1), (2), and (3): Reacting flow of n-butane/air mixture at stoichiometry

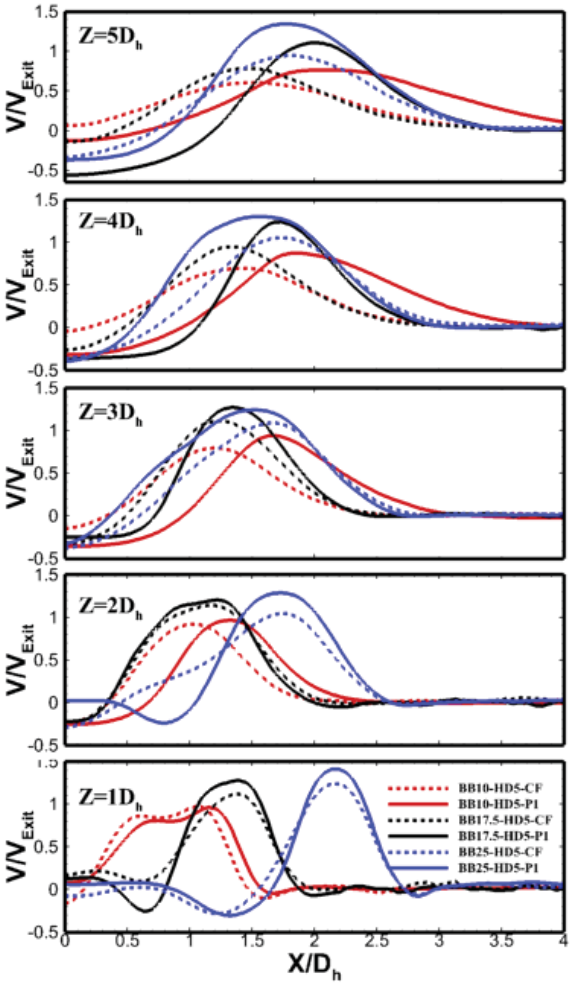

Fig. 6 Normalised time-averaged axial velocity profile at the different axial locations for different experimental conditions

B. Velocity Fields Comparison for Isothermal and Reacting Flows

Fig. 6 shows the time-averaged radial profile of normalized axial velocity at different axial locations of isothermal/ reacting flows. The uncertainty was estimated [2] as 2.36% of the area-averaged exit velocity (V_{Exit}) for all the cases. Isothermal and reactive flow patterns were nearly the same. At $Z = 1D_h$, the figure shows that the axial velocity was negative behind the BB, indicating that the wake zone was evident in burners with larger bluff body diameters at both isothermal/reacting flows. For BBD = 10 mm, the bluff body effect was negligible as the negative value of the velocity was absent due to a higher nozzle exit cone angle, which caused the flow to converge. Near the exit, the radius at which the transition of axial velocity from negative to positive indicates the size of BB-RCZ. It also indicated that the peak velocity hiked, and its location shifted radially outwards with an increase in the BB size at all reported axial distances for both the isothermal/reacting flow cases.

At BBD = 25 mm, the peak velocity shifted inwardly towards the axis due to the convergent nature of the burner exit till $Z = 3D_h$, and later it shifted outwards due to the CRCZ. The decay in the magnitude of the velocity was quicker in cold flows, whereas it was slower in reacting flows due to the energy added by combustion gases' rapid expansion and flow acceleration due to density difference. The peak axial velocity at $Z = 5D_h$ was reduced to 79.6%, 86.6%, and 95.4% of its counterpart at $Z = 1D_h$ for BBD of 10 mm, 17.5 mm and 25 mm. The power rating was higher at larger BB sizes, and the velocity reduction was not that severe within the considered distances. The flow field acceleration at the reaction zone was quite common and was reported in [4].

C. Jet Spreading Rate

Fig. 7 depicts the spreading rate of a free swirling jet from the current burner at Re = 4000 as a function of the increase in burner nozzle annular area for isothermal flow and hot flow cases. The jet spread angle was calculated by the procedure mentioned in [11]. For isothermal/hot flow cases, the half-width jet angles for various bluff body sizes such

TABLE II
OPERATING CONDITIONS FOR DIFFERENT TEST CASES

Sl.No	Burner	ϕ	Bluff Body Dia. (mm)	Hydraulic Dia.(mm)	m_{Air} (SLPM)	m_{Fuel} (SLPM)	Power Rating (KW)	Exit Velocity (m/s)
1	BB10-HD5-P1	1	10 ($2D_h$)	5	71.7	2.3	4.3	12
2	BB17.5-HD5-P1	1	17.5 ($3.5D_h$)	5	114.5	3.66	6.8	12
3	BB25-HD5-P1	1	25 ($5D_h$)	5	157.5	5.07	9.5	12

as 100%, 160% and 220% are 10°/34°, 8°/26°, and 6°/22° respectively. In the present axial swirl burner, the spreading angle or divergence in the jet decreased roughly linearly with an increase in annular area (S1.5) for the hot flow instances, while for the isothermal flow, the jet spread rate dropped at a lower rate compared to the hot flow cases, which was due to the higher flow momentum with an increase in the annular area. When the isothermal and hot flow situations are compared, it is clear that the flame, not the flow's swirling motion, mostly causes the divergence [3].

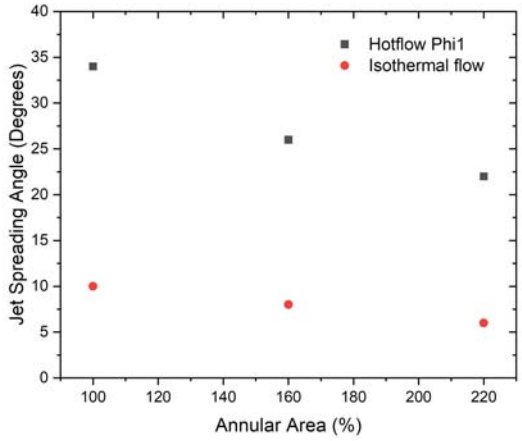

Fig. 7 Jet spreading angle (α1/2) for different burner exit annular areas

D. Recirculation Zone

Fig. 8 displays the axial profile of time mean centre line axial velocity normalised by the mean exit velocity at both the isothermal/reacting conditions. The appearance of negative axial velocity values indicated the existence of RCZs. The length of the RCZ (L) was the axial height from the exit of the burner at which the centerline axial velocity transited from negative to positive. The estimated recirculation lengths for BB10-HD5-P1, BB17.5-HD5-P1, and BB25-HD5-P1 were $4.52D_h$, $6.78D_h$, and $8.73D_h$, respectively. For the corresponding isothermal cases, the estimated recirculation lengths were $3.6D_h$, $5.28D_h$, and $9.8D_h$, respectively. The presence of the reaction zone and the higher momentum of the products due to thermal expansion hiked the magnitude of the negative velocity and the recirculation length, irrespective of an increase in the viscosity of the products. In isothermal flows, the momentum is low; hence, the CRCZ is smaller. But for the higher bluff body reacting case, the vortex shedding from the wake region pushed the CRCZ further downstream compared to the corresponding isothermal case hence the recirculation length is lower for the reacting case for the higher bluff body burner. Following [20], the mass flow rate reversed into the RCZ was calculated and normalised using (2):

$$\frac{\dot{m}_r}{\dot{m}_o} = \frac{\int_0^r 2\pi\rho u r dr}{\dot{m}_o} \tag{2}$$

where r denotes the RCZ's width. The normalised reversed mass flow rate was estimated at the axial distance where the negative value of the axial velocity attained the peak value. For all isothermal flows, the normalised reverse mass flow rate was calculated. The predicted normalised reverse mass flow rates for bluff body size 10 mm, 17.5 mm, and 25 mm are 0.0086, 0.0201, and 0.0245, respectively. The mass reversed into the RCZ is greater for larger bluff bodies than for smaller bluff bodies. According to this, an increase in exit annular area, i.e., a 120% increase in annular area, virtually tripled the value of reversed mass flow rate for the current burner design at a given Reynolds number.

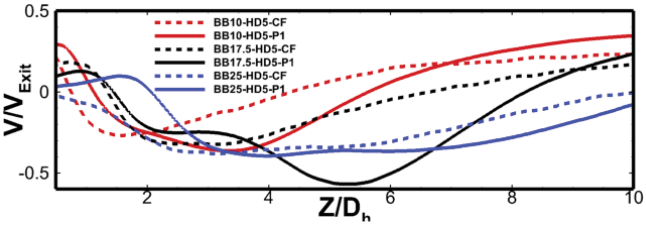

Fig. 8 Normalized time averaged centerline axial velocity profile for different exit annular area of isothermal and hotflow cases

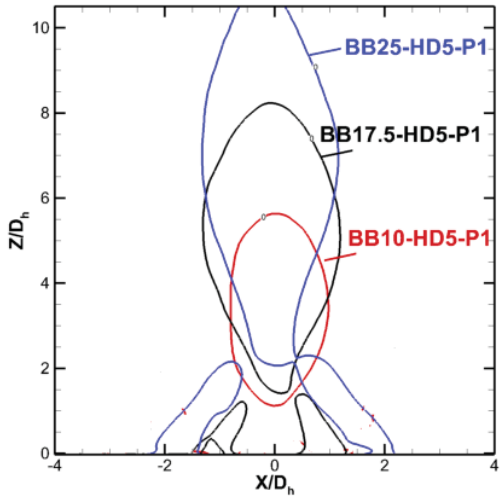

Fig. 9 Normalized shape of the RCZ defined by the iso-line of zero axial velocity for different burner annular exit area cases at stoichiometry

Fig. 9 demonstrates the normalized central RCZ lengths

with a hydraulic diameter of the premixed stoichiometric n-butane – air flames at various sizes of the bluff body. The length of the RCZ was linearly varying with an increase in the cross-sectional area of the bluff body. As demonstrated by Fig. 9, where the swirl intensity (S) was constant at 1.5, and at stoichiometric conditions, the normalized CRCZ width (W/D_h) was 2.32 for all the investigated burner exit areas. It can be concluded that the CRCZ width is strongly dependent only on the swirl intensity and not on the burner exit configuration, which was also reported by [6]. The wake region behind the bluff body was observed for higher bluff body sizes, and the size of the BB-RCZ grew wake region along with the bluff body size. For larger BB sizes, the BB-RCZ grew larger and began to interact with the CRCZ and enhanced the turbulence intensity.

E. Turbulent Kinetic Energy

Fig. 10 shows the distribution of turbulent kinetic energy along the centerline for different burner exit geometries at both the isothermal/reacting flow conditions. This was essential to comprehend the turbulence generated in the flow field due to a variation in the burner exit/bluff body area. The turbulent kinetic energy was estimated as follows:

$$TKE = 0.5(u'^2 + v'^2) \tag{3}$$

where v′ and u′ represented the RMS fluctuation velocities in the axial and radial direction, respectively. Fig. 10 demonstrates that the TKE of the burner with the smallest bluff body was quite high at the exit of the burner at both the isothermal/reacting flow conditions due to the strong flow acceleration affected by the exit convergent nozzle geometry of the swirl burner. Slightly away from the same burner, the TKE decreased as the flow field diverged due to the swirling flow in both cases. In reacting flows, the TKE in the centreline was lower than its isothermal counterparts due to the higher viscosity of the hot combustion products. The interesting observation was that the burner with a bluff body diameter of 17.5 mm had the highest TKE as compared to other burners having BBD of 10 mm and 25 mm, indicating that this burner geometry generated the highest turbulence, due to which the flame anchored very close to the burner exit represented by the smallest TKE at the reacting flow conditions. In the burner with 25 mm BB, the flow diverges from the burner exit resulting in lower TKE as is not the case with other burners, and the reaction surface was also attached to the burner exit resulting in further lower TKE.

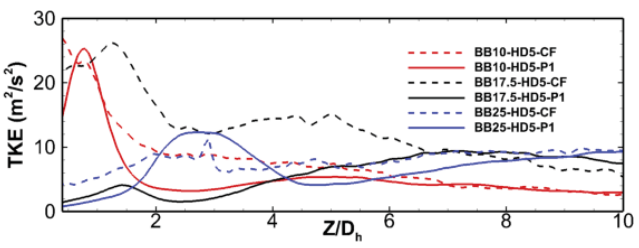

Fig. 10 Turbulent kinetic energy along the centerline

The contours in Fig. 11 depict the planar distribution of TKE for three different burner exit areas necessary to understand the reason behind the stabilization of premixed n-butane-air flames. It shows that, for isothermal flows, the high turbulence activity was confined in the core region of the wake flow and the shear layer due to the large velocity gradient [9]. The shear layer between the annular flow and the RCZ area exhibited the peak TKE in reacting flow cases. The fact that the shear layer consistently has the largest TKE is a characteristic of all swirl burners. In contrast to their isothermal counterparts, the distribution of turbulence intensity levels in reacting flows has a distinct tendency. According to [9], the high mean velocity across the oblique wrinkled flame front caused a rise in the turbulence kinetic energy. Additionally, it was discovered that the turbulence level decreased in the RCZs. The flow turbulence was reduced in RCZ essentially due to the presence of hot combustion products with high temperatures having larger viscosity and undergoing dilatation. The decrease in turbulence was prominently due to an increase in the viscosity in the RCZ [5]. The maximum turbulent kinetic energy is found at the reaction zone of BB17.5-HD5-P1, which, in contrast to the other two cases, boosted mixing and entrainment, as shown in Fig. 11.

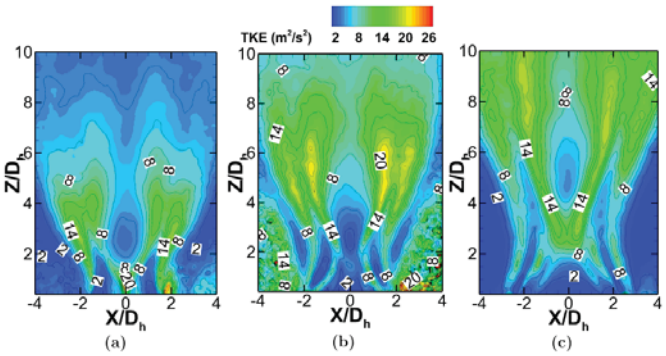

Fig. 11 Turbulent kinetic energy contour of reacting flow cases (a) BB10-HD5-P1, (b) BB17.5-HD5-P1, (c) BB25-HD5-P1

F. Integral Length Scale

The integral length (l) scale was estimated by following [11]. Knowledge of the length scale is essential to categorize the premixed turbulent flames. The variations in normalized length scale along the normalized axial distance for distinct burner exit annular areas are depicted in Fig. 12. Integral length scale values for BB10-HD5-P1 ranged from 0.5Dh to $0.7D_h$. The integral length scale over the axial distance for BB17.5-HD5-P1 varies between $0.38D_h$ and $0.65D_h$. The integral length scale for BB25-HD5-P1 varies between $0.45D_h$ and $0.7D_h$. The only degree of freedom that varied was the annular exit area of the burner, while the flow and thermodynamic parameters were the same. Fig. 12 shows that the ILS were smaller, close to the burner exit for all the studied cases and gradually increased in the downstream section of the burner exit. This was essentially due to the flow widening.

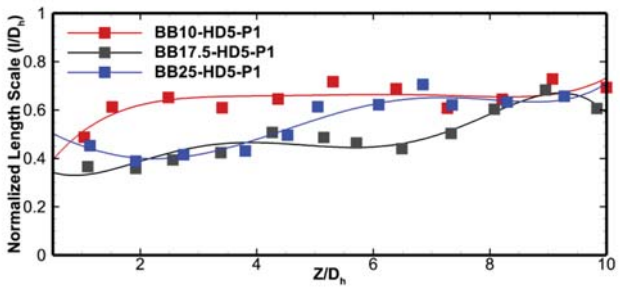

Fig. 12 Normalized integral length scale vs. normalized axial distance for different nozzle annular areas

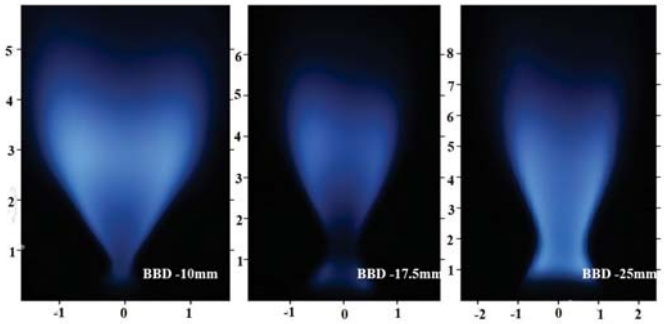

Fig. 14 Direct photography of flames at stoichiometry for different nozzle annular areas

G. Lean Blowout

LBO was essential to understand a burner's lower flammability limit (LFL). It was executed by anchoring a stoichiometric flame at the desired Reynolds number. Then, only the fuel flow rate gradually decreased until the flame was extinguished. Unexpectedly, the equivalence ratios at which LBO was achieved for BB10-HD5-P1, BB17.5- HD5-P1, and BB25-HD5-P1 were 0.80, 0.92 and 0.82, respectively. The LFL of a burner with BBD = 17.5 mm was quite narrow due to: (a) it has the highest TKE, as explained in the previous section, (b) it resulted in more air entrainment, and (c) higher flame stretching.

Fig. 13 depicts the inverse Abel transform of planar CH* distributions of the measured chemiluminescence intensities of a stoichiometric n-butane air turbulence flame at different burner nozzle exit annular regions. It indicated that the chemiluminescence intensity was significantly lower in the BB17.5-HD5-P1 case, confirming the higher level of air entrainment into the reaction zone.

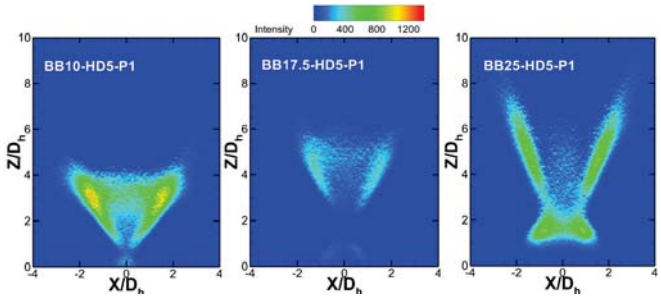

Fig. 13 Inverse Abel transform of CH* chemiluminescence for different nozzle annular areas

The time-averaged direct photograph of a flame was displayed in Fig. 14. The axes of Fig. 14 were normalised by a factor of 10. The axial length of the BB17.5-HD5-P1 and BB10-HD5-P1 case flames were nearly the same irrespective of flow momentum, indicating that the BB17.5-HD5-P1 case had stronger mixing of ambient air with the reaction zone. This can be corroborated by the lower level of the overall luminosity of the BB17.5-HD5-P1 case.

IV. Conclusion

This study investigated the impact of a swirl burner's increase in the annular exit area (S = 1.5) on the stabilization of premixed turbulent flames. The study was conducted at both isothermal and reacting flow conditions at Re = 4000. Planar PIV was used to measure the velocity fields. OH* chemiluminescence was measured to locate the reaction zone. Under isothermal and hot flow conditions, the PIV approach measured the two-dimensional velocity field. In all cases, either one or two RCZs were detected. As the burner exit area increased, the recirculation width and length increased due to an increase in the overall momentum. The measured TKE of the reacting cases was the largest for the BB17.5-HD5-P1 burner, resulted in higher fluctuating surface area, enhanced air entrainment, improved mixing between reactants and burned products, smaller flame size and weaker flame luminosity. The LBO was measured, and the burners with 100% and 220% annular exit area fared better than the 160% case. At the 160% case, the LBO occurred close to the stoichiometric condition due to higher turbulence and stronger entrainment of ambient air.

Acknowledgment

We sincerely thank the Department of Space, India for their financial support.

References

[1] J Beer. "M. and Chigier, NA, Combustion Aerodynamics". In: *Appl. Sci. Publ. LTD* (1972).

[2] RG Jr Bill and K Tarabanis. "The effect of premixed combustion on the recirculation zone of circular cylinders". In: *Combustion science and technology* 47.1-2 (1986), pp. 39–53.

[3] CK Chan et al. "Freely propagating open premixed turbulent flames stabilized by swirl". In: *Symposium (International) on Combustion*. Vol. 24. 1. Elsevier. 1992, pp. 511–518.

[4] Nehemiah A Chigier and Amnon Chervinsky. "Aerodynamic study of turbulent burning free jets with swirl". In: *Symposium (International) on Combustion*. Vol. 11. 1. Elsevier. 1967, pp. 489–499.

[5] Cecile Cohe et al. "CO2 addition and pressure effects on laminar and turbulent lean premixed CH4 air flames". In: *Proceedings of the Combustion Institute* 32.2 (2009), pp. 1803–1810.

[6] Fabio Cozzi, Aldo Coghe, and Rohit Sharma. "Analysis of local entrainment rate in the initial region of isothermal free swirling jets by stereo PIV". In: *Experimental Thermal and Fluid Science* 94 (2018), pp. 281–294.

[7] Irvin Glassman, Richard A Yetter, and Nick G Glumac. *Combustion*. Academic press, 2014.

[8] Ashwani K Gupta, David G Lilley, and Nick Syred. "Swirl flows". In: *Tunbridge Wells* (1984).

[9] MR Johnson et al. "A comparison of the flowfields and emissions of high-swirl injectors and low-swirl injectors for lean premixed gas turbines". In: *Proceedings of the Combustion Institute* 30.2 (2005), pp. 2867–2874.

[10] Kim et al. *Application of Thermo-Fluidic Measurement Techniques: An Introduction*. Butterworth-Heinemann, 2017.

[11] Hanzhuang Liang and T Maxworthy. "An experimental investigation of swirling jets". In: *Journal of fluid mechanics* 525 (2005), pp. 115–159.

[12] Muammer Ozgoren. "Flow structure in the downstream of square and circular cylinders". In: *Flow Measurement and Instrumentation* 17.4 (2006), pp. 225–235.

[13] Rodolphe Perrin et al. "Near-wake turbulence properties in the high Reynolds number incompressible flow around a circular cylinder measured by two-and three-component PIV". In: *Flow, turbulence and combustion* 77.1 (2006), pp. 185–204.

[14] C Prathap, R Manikandan, and R Sadanandan. "Experimental Investigation on the Effects of Swirl on the Exit Turbulent Flow Field of an Unconfined Annular Burner at Isothermal and Reacting Conditions". In: *Journal of Applied Fluid Mechanics* 13.3 (2019), pp. 839–847.

[15] A Rowhani et al. "Effects of the bluff-body diameter on the flow-field characteristics of non-premixed turbulent highly-sooting flames". In: *Combustion Science and Technology* 194.2 (2022), pp. 378–396.

[16] RW Schefer et al. "Effect of confinement on bluff-body burner recirculation zone characteristics and flame stability". In: *Combustion science and technology* 120.1-6 (1996), pp. 185–211.

[17] Haojie Tang et al. "Characteristics of flame modes for a conical bluff body burner with a central fuel jet". In: *Journal of engineering for gas turbines and power* 135.9 (2013).

[18] AMKP Taylor and JH Whitelaw. "Velocity characteristics in the turbulent near wakes of confined axisymmetric bluff bodies". In: *Journal of fluid mechanics* 139 (1984), pp. 391–416.

[19] Yiheng Tong et al. "Effects of the position of a bluff-body on the diffusion flames: A combined experimental and numerical study". In: *Applied Thermal Engineering* 131 (2018), pp. 507–521.

[20] Koen P Vanoverberghe, Eric V Van Den Bulck, and Mark J Tummers. "Confined annular swirling jet combustion". In: *Combustion Science and Technology* 175.3 (2003), pp. 545–578.